Fermilab

Fermi National Accelerator Laboratory
P.O. Box 500 • Batavia, Illinois • 60510

TD-97-040
September 30, 1997

Magnetic Field Analysis of HGQ Coil Ends

G. Sabbi

Abstract:
In this note a magnetic field analysis of the of the HGQ baseline design for the end regions is presented. This design is implemented in the first HGQ short model, HGQS01.

1 Introduction

The first design iteration of the HGQ coil ends consisted of a magnetic optimization of the position of the conductor groups in the return end [1], based on which a mechanical optimization of both the return and the lead end geometry was carried out using program BEND [2, 3]. The magnetic properties of the resulting design have been investigated in the course of several studies which separately addressed the issues of peak field in the coil [4], Lorentz forces [5], and field quality [6]. In this note, a new magnetic analysis of the HGQ coil ends is presented. The calculations have been performed using ROXIE [7]. The model has been defined using the recently developed BEND-ROXIE interface. The purpose of this analysis is to compare the results obtained with the new method with the previous ones, and to provide a global discussion of the different aspects of the baseline HGQ end design, which has been adopted for the HGQS01 model.

2 Computer model

Figure 1 and 2 show the longitudinal cross-section at the pole angle of the HGQ return and lead end. In each case, the origin of the z-axis is chosen as defined in [2]. The z-axis is directed outwards from the magnet body. The iron yoke starts at z=-15 cm for the lead end, at z=-5 cm for the return end. In the lead end, the splice ramp starts at z=-13.78 cm for both the inner and the outer coil.

The 3D model for the coil end regions is built by extrusion along the z axis, starting from a 2D model of the magnet cross-section. For the return end, which has exact quadrupole symmetry, it is sufficient to define the cross-section of one octant of the magnet, as shown in figure 3. Both the blocks and the conductors are numbered from the mid-plane side to the pole side, starting with the outer layer. The ROXIE block/conductor definitions and the BEND definitions for the corresponding conductor groups are reported in table 1. These definitions apply to both the return end and the magnet body.

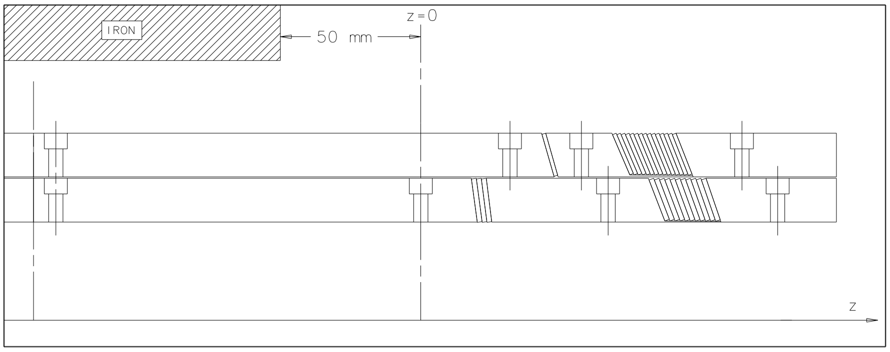

Figure 1: HGQ return end geometry

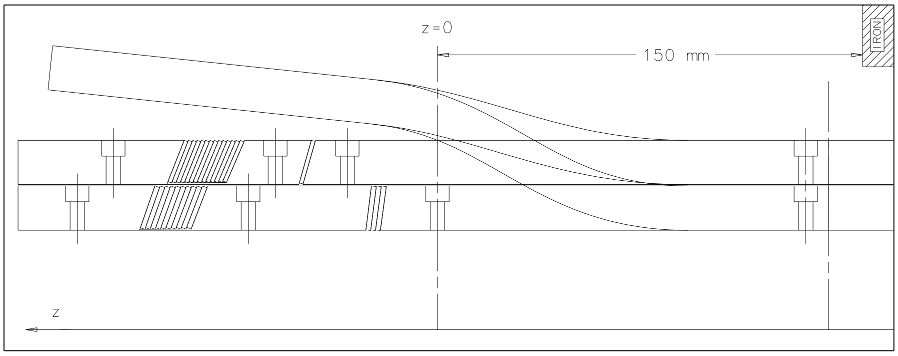

Figure 2: HGQ lead end geometry

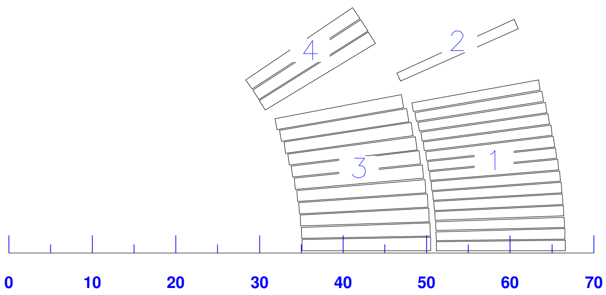

Figure 3: Coil cross-section model for the HGQ return end. Axis scale is in mm.

ROXIE		BEND	No. turns	Description
Block #	Turn #	Group		
1	1 to 15	q2or312	15	2^{nd} wound, outer
2	16	q1or01	1	1^{st} wound, outer
3	17 to 27	q2ir29	11	2^{nd} wound, inner
4	28 to 30	q1ir03	3	1^{st} wound, inner

Table 1: Block and turn definitions for the HGQ return end. The same definitions apply in the magnet body.

The data for the 3D extrusion is obtained by reading into the ROXIE program the BEND coordinates files which specify the cross-sections of each conductor at small intervals along z. For the return end, 20 cross-sections have been specified from the edge of the iron yoke to the coil termination. The cross-sections are spaced more closely in those regions where the bending radius is smaller. Once the 3D geometry of the octant is specified, symmetry operations are applied automatically by ROXIE to define the entire magnet: the resulting geometry for the return end is shown in figure 4. A straight section extending from the edge of the iron yoke for 1.5 m in the negative z direction is also included in the model.

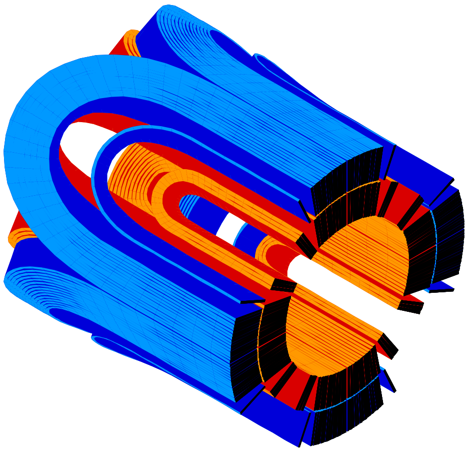

Figure 4: ROXIE-BEND model for the HGQ return end (only the part of the coil extending beyond the edge of the iron yoke is shown).

For the lead end, where the coil is not symmetric with respect to the pole plane, it is necessary to define both the left and the rigth side of each quadrant (coil). The 2D cross-section used as a basis for the extrusion is shown in figure 5. In each layer, the blocks and conductors are numbered from the midplane to the pole, starting from the left side of the coil (as seen by an observer looking towards the positive z direction). The ROXIE block/conductor definitions and the BEND definitions for the corresponding conductor groups are reported in table 2.

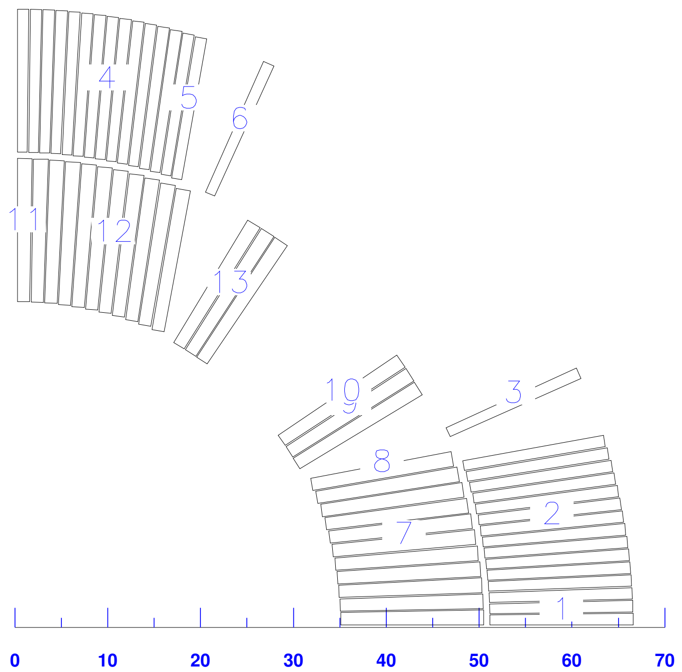

Figure 5: Coil cross-section model for the HGQ lead end. The axis scale is in mm.

ROXIE				BEND	No. turns	Description
Blk	Turn	Conn. blk	End type	Group		
1	1		1		1	Straight to quadrant splice
2	2 to 15	4	2	q2ol311	14	2^{nd} wound, outer, left
3	16	5	3	q1or01	1	1^{st} wound, outer, left
4	17 to 30	2	7	q2ol212	1	2^{st} wound, outer, right
5	31	3	8	q1ol01	1	2^{st} wound, outer, right
6	32	10	12	qoa/b	1	Ramp to coil spilce (outer)
7	33 to 42	12	4	q2il19	10	2^{nd} wound, inner, left
8	43	13	5	q1il01	1	2^{nd} wound, inner, left
9	44 to 45	13	6	q1il02	2	1^{st} wound, inner, left
10	46	6	13	qia/b	1	Ramp to coil splice (inner)
11	47		9		1	Straight to quadrant splice
12	48 to 57	7	10	q2il28	10	2^{nd} wound, inner, right
13	58 to 60	8,9	11	q1ir03	3	1^{st} wound, inner, right

Table 2: Block and turn definitions for the HGQ lead end.

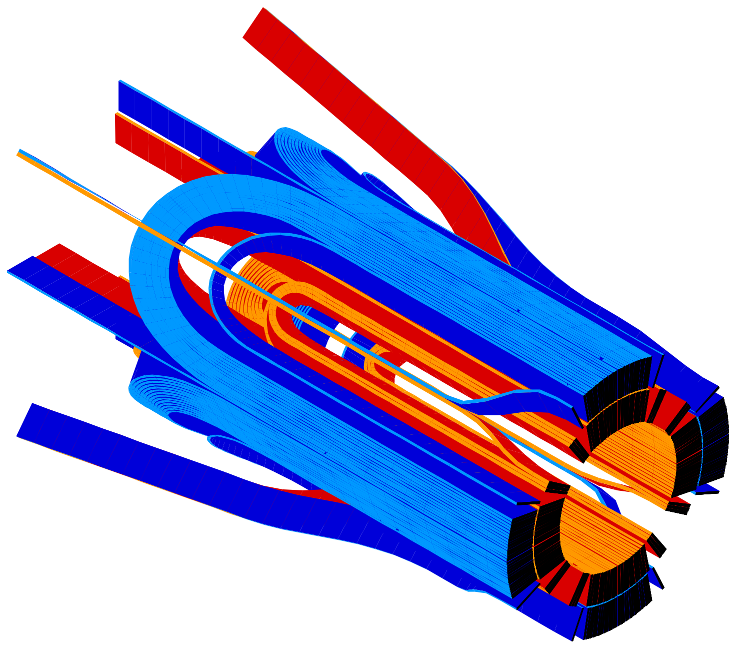

Figure 6: ROXIE-BEND model for the HGQ lead end (only the part of the coil extending beyond the edge of the iron yoke is shown).

For the lead end 3D extrusion, 30 cross-sections have been specified from the edge of the iron yoke to the coil termination. The resulting geometry is shown in figure 6. The model also includes a straight section extending from the edge of the iron yoke for 1.5 m in the negative z direction. The coil to coil splice length is 11.43 cm. The quadrant splices are not included in the model; for each coil, the two connection conductors extend straight from the magnet body in the z direction and are truncated at z=15 cm.

The field calculation is based on the Biot-Savart law. The iron yoke is regarded as a magnetic mirror of circular shape (inner radius 9.256 cm) with infinite permeability. For the ROXIE calculation, each conductor has been subdivided in current filaments, one for each strand. The total number of strands is 38 in the inner layer, 46 in the outer layer. For both the lead and the return end calculations, a straight section extending in the negative z direction for 1.5 m from the start of the iron yoke towards the magnet body has been assumed.

3 Peak field

For the 3D peak field calculation, the method implemented in ROXIE does not allow to take into account the contribution of the iron yoke. This means that the field values calculated in the proximity of the edge of the iron yoke (z=-50 mm for the return end, z=-150 mm for the lead end) are incorrect. However, the actual peak field normally occurs close the coil termination, and previous calculations [1] show that the distance from the edge of the iron yoke to this region is sufficiently large to ensure that the contribution of the iron yoke can be neglected.

Return end			Lead end		
Block #	Turn #	B^{max}/I T/kA	Block #	Turn #	B^{max}/I T/kA
1	15	0.599 (0.611)	1	1	0.419
2	16	0.541 (0.540)	2	15	0.576
3	27	0.599 (0.598)	5	31	0.556
4	30	0.656 (0.656)	6	32	0.401
			8	43	0.597
			10	46	0.639
			11	47	0.566
			12	56	0.588
			13	60	0.639

Table 3: Field load line coefficients in the lead and return end regions. The numbers in parenthesis are from [4] and are reported for comparison.

Block #	Turn #	B^{max}/I (T/kA) I=1kA	I=14kA
1	15	0.596	0.576
2	16	0.588	0.567
3	27	0.649	0.631
4	30	0.707	0.687

Table 4: Field load line coefficients in the magnet body, at low and high current [4].

The linear coefficients for the maximum field in each block of the lead and return end as function of current are reported in table 3. The numbers in parenthesis are from [4]: a good agreement is generally observed, with some differences due to the use of a higher number of current filaments (one for each strand) in the new calculation and to an improved modelling of the coil geometry made possible by the new BEND-ROXIE interface. The corresponding coefficients calculated in the magnet body (taking into account the iron saturation and the detailed iron cross-section) are reported in table 4. A comparison between these values shows that the peak field in the first-wound block of the outer layer (block 1) is higher in the return end than in the magnet body. This factor limits the magnet performance and constitutes a serious drawback to the present HGQ end design.

Figure 7 shows the variation of the magnetic field along the z coordinate for some relevant conductors of the return end. For each block, the conductor where the maximum field occurs has been chosen. As can be seen, the behaviour of block 1 is anomalous in the sense that the field keeps increasing all the way until the coil termination, while for the other conductor groups a peak is reached in the area where the conductors start bending, then the field starts to decay. This unusual behaviour can be explained by an enhancement of the local field at the position of conductor 16 due to the relative positions of block 1 (outer layer) and block 3 (inner layer), as shown in figure 8.

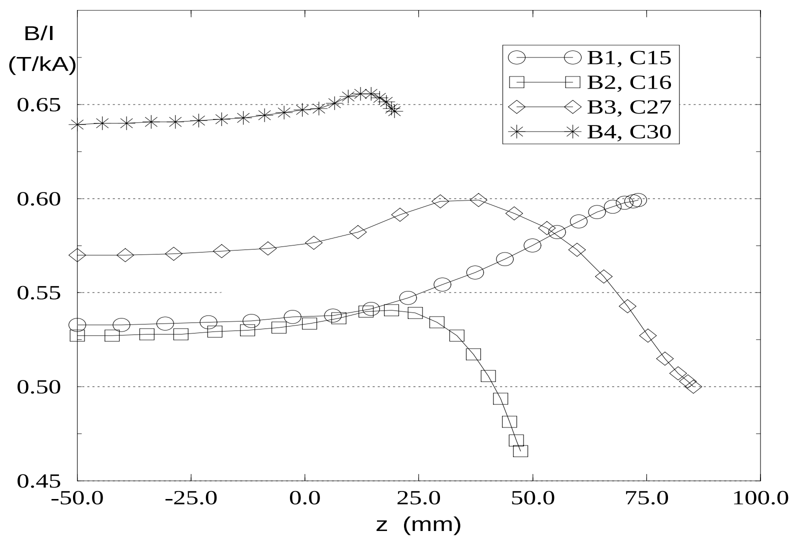

Figure 7: Field load line along z for some conductors in the return end. For each block, the conductor where the maximum field occurs has been chosen.

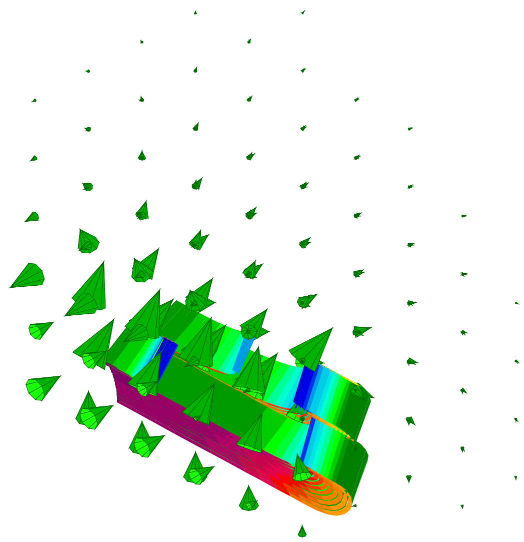

Figure 8: Magnetic field enhancement at the position of conductor 16 resulting from a constructive interference of the contributions of block 1 and block 3.

The variation of the magnetic field along the z coordinate for the most relevant conductors of the lead end is shown in figure 9 (outer layer) and 10 (inner layer). It can be seen that the peak field enhancement at the position of conductor 15 is still present, however the actual value is lower here than in the return end (0.576 T/kA instead than 0.599 T/kA). This can be explained by the fact that in the lead end both second-wound groups have one less conductor than in the return end. No particular problem arises in the inner layer, as well as at the location of the splice ramps and current leads.

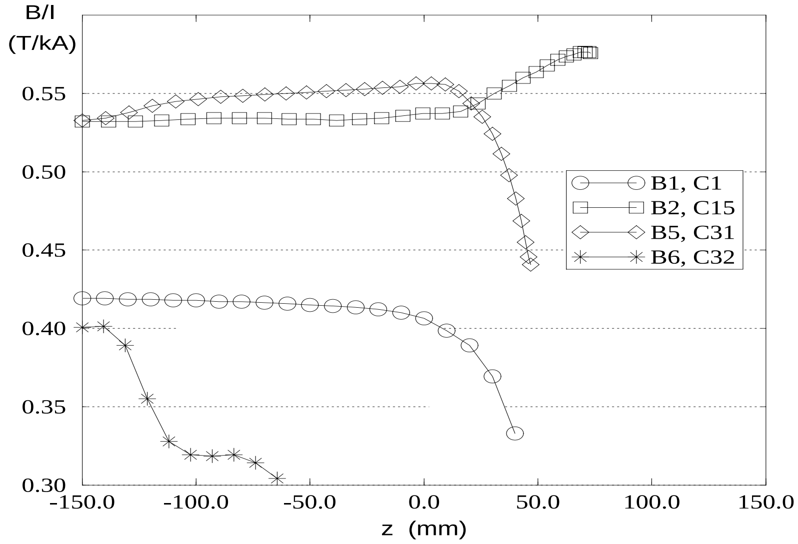

Figure 9: Field load line along z for relevant blocks/conductors in lead end (outer layer).

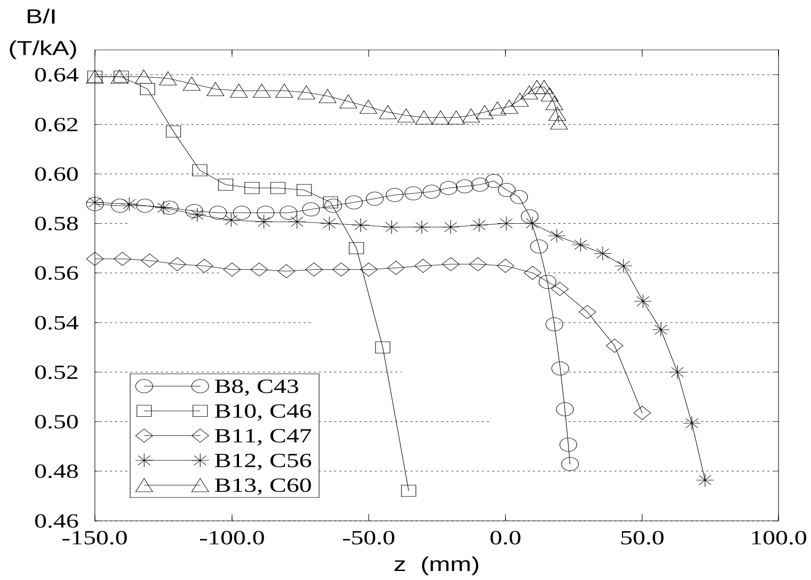

Figure 10: Field load line along z for relevant blocks/conductors in lead end (inner layer).

4 Lorentz forces

The Lorentz forces acting on the coil windings depend quadratically on the excitation current. The F/I^2 coefficients for the return end are reported in table 5. These values are for the left side only: the forces are symmetric with respect to the pole plane, i.e. $F_x^r = F_y^l$, $F_y^r = F_x^l$, $F_z^r = F_z^l$.

Block	Description	x	y	z
1,2	Outer layer, left	-119	-512	127 (128)
3,4	Inner layer, left	605	-374	55 (54)

Table 5: Coefficients for the Lorentz forces (N/kA^2) in the return end (one octant). The numbers in parenthesis are from [5] and are reported for comparison.

Block	Description	x	y	z
1,2,3	Outer layer, left	-233	-897	119
4,5	Outer layer, right	-825	-251	122
7,8,9	Inner layer, left	1007	-638	57
11,12,13	Inner layer, right	-718	1077	51
6	Outer layer ramp/splice	58	44	8
7	Inner layer ramp/splice	65	-70	4

Table 6: Coefficients for the Lorentz forces (N/kA^2) in the lead end. Values are given for the left and the right side of one quadrant of the magnet. The coefficients for the inner and outer coil ramp/splices have been singled out.

Block	Description	Without iron yoke		With iron yoke	
		x	y	x	y
1,2	Outer layer, left	-1.212	-3.961	0.224	-4.236
3,4	Inner layer, left	4.992	-3.469	5.870	-3.731

Table 7: Coefficients for the Lorentz forces per unit length and current in the HGQ straight section (N/mm/kA^2) These values are for one octant of the magnet. The iron yoke is regarded as a magnetic mirror with infinite permeability and inner radius 9.2564 cm.

The coefficients for the forces in the lead end are reported in table 6. For both return and lead end, the forces are given for the section starting from the edge of the iron yoke (z=-5 cm for the return end, z=-15 cm for the lead end) until the coil termination. For the longitudinal forces in the return end, a good agreement is obtained with respect to the result from [5]. The contribution of the section of the coil from the edge of the iron yoke to z=0 can be singled out by using the coefficients for the transverse forces per unit length in the magnet straight section when no iron yoke is present, reported in table 7. In particular, the contribution of conductor #16 (outer coil splice ramp) is 0.088 N/mm/kA^2 in the x direction, -0.445 N/mm/kA^2 in the y direction, while the contribution of conductor #30 (inner coil splice ramp) is 0.395 N/mm/kA^2 in the x direction, -0.446 N/mm/kA^2 in the y direction. Note that all values are given for the left side of the coil, while the inner coil splice ramp is located on the right side. The coefficients for the transverse forces in the magnet body are also reported for comparison in table 7.

5 Field quality

In the straight section of the magnet, where translational symmetry applies and the longitudinal component of the magnetic field vanishes, the magnetic field in the bore can be represented in terms of multipole coefficients defined according to the following expression:

$$\begin{aligned} B_\theta(r,\theta) &= \sum_{n=1}^{\infty} \left(\frac{r}{r_0}\right)^{n-1} (B_n \cos n\theta + A_n \sin n\theta) \\ B_r(r,\theta) &= \sum_{n=1}^{\infty} \left(\frac{r}{r_0}\right)^{n-1} (-A_n \cos n\theta + B_n \sin n\theta) \end{aligned}$$

The same multipole coefficients appear in the equivalent expansion in complex notation:

$$B_y(x,y) + iB_x(x,y) = \sum_{n=1}^{\infty} (B_n + iA_n) \left(\frac{x+iy}{r_0}\right)^{n-1} \tag{1}$$

Here r_0 is a reference radius, which should be comparable to the transverse dimension of the beam. A typical choice is about 2/3 of the inner-bore radius of the coil (about 23 mm for the HGQ). However, since the field harmonics for LHC magnets, including the quadrupoles of the inner triplet, are given at a reference radius r_0 of 1 cm, the same value will be used here.

The B_n and A_n parameters are usually referred to as normal and skew harmonic coefficients. For a quadrupole magnet, it is often convenient to express the multipole components in "units" of 10^{-4} of the main quadrupole field B_2:

$$b_n = B_n/B_2 \cdot 10^4$$

$$a_n = A_n/B_2 \cdot 10^4$$

In the magnet end regions the transverse field can in general depend on z and the longitudinal field component does not vanish. In this case, additional terms (pseudo-multipoles) are required in the expansion for the local field [8]. A simpler expansion based on equation 1 can however be recovered for the integral of the transverse field, provided that the longitudinal field component vanishes at the boundaries of the integration interval. In this case, the pseudo-multipole components must integrate to zero and can therefore be eliminated [8]. This condition is satisfied if the integral covers the whole end region, i.e. if the starting point z_p is sufficiently inside the magnet body and the end point z_q is sufficiently far away from the coil termination. The integrated harmonics are then calculated according to the following expression:

$$\int_{z_p}^{z_q} [B_y(x,y,z) + iB_x(x,y,z)]dz = \sum_{n=1}^{\infty} (\hat{B}_n{}^{[z_p,z_q]} + i\hat{A}_n{}^{[z_p,z_q]}) \left(\frac{x+iy}{r_0}\right)^{n-1} \tag{2}$$

As in the magnet straigth section, it is convenient to express the integrated multipole components $\hat{B}_n$, $\hat{A}_n$ in the end regions in "units" of 10^{-4} of the main integrated quadrupole field $\hat{B}_2^{[z_p,z_q]}$:

$$\hat{b}_n^{[z_p,z_q]} = \frac{\hat{B}_n^{[z_p,z_q]}}{\hat{B}_2^{[z_p,z_q]}} \cdot 10^4 \tag{3}$$

$$\hat{a}_n^{[z_p,z_q]} = \frac{\hat{A}_n^{[z_p,z_q]}}{\hat{B}_2^{[z_p,z_q]}} \cdot 10^4 \tag{4}$$

The magnetic length L_m of the interval $[z_p, z_q]$ is defined as the length of straigth section which would provide an equivalent integrated strength for the main (quadrupole) field component:

$$L_m^{[z_p,z_q]} = \frac{\hat{B}_2^{[z_p,z_q]}}{B_2} \tag{5}$$

For the present study, the integrated multipoles have been obtained from 50 line integrals of the transverse field, calculated along lines parallel to the z-axis, at the reference radius of 1 cm and equally spaced azimuthal angles. The integration limits are [-25,+25] cm for the return end and [-35,+25] cm for the lead end. The longitudinal component of the magnetic field at the boundaries of the integration intervals is negligibly small. Each field integral has been evaluated by adding up the contributions calculated at 1 mm intervals along z. The magnetic length calculation is based on a transfer function in the magnet body of 18.22 T/m/kA, as obtained for a 2D analysis carried out under the same assumptions (conductors aligned to the coil outer radius, circular iron yoke of inner radius 9.2564 cm and infinite permeability) [4]. The results for the magnetic length and the average multipole components in the HGQ return and lead end regions are reported in table 8 and 9.

In order to carry out a beam tracking analysis where the local variation of the field is taken into account, a 3D expansion for the local (longitudinal and transverse) field in terms of pseudo-multipoles is needed. This expansion can be built starting from the field values $\vec{B}(r_0, \theta_i, z_j)$ calculated on a cylindrical surface inside the magnet bore [9]. These data have been calculated for $r_0 = 1$ cm, at 50 different angles and 1 mm longitudinal spacing, and are available upon request.

L_m (cm)	31.78
$\hat{b}_2$	10000
$\hat{b}_6$	0.048
$\hat{b}_{10}$	-0.0041
$\hat{b}_{14}$	-0.000017

Table 8: Integrated harmonic coefficients for the return end. The integration interval starts at $z = -25$ cm and ends at z=+25 cm.

L_m (cm)	40.72
$\hat{b}_2$	10000
$\hat{b}_6$	0.597
$\hat{b}_{10}$	-0.0032
$\hat{b}_{14}$	-0.000015
$\hat{a}_2$	42.8
$\hat{a}_6$	0.025
$\hat{a}_{10}$	-0.0011
$\hat{a}_{14}$	0.000006

Table 9: Integrated harmonic coefficients for the lead end. The integration interval starts at z=-35 cm and ends at z=+25 cm.

Parameter	2D analysis	Return end	Lead end
Tranfer function (T/m/kA)	18.22	18.22	18.22
b_2	10000	10000	10000
b_6	-0.0016	-0.0016	-0.0016
b_{10}	0.000048	0.00048	0.000050
b_{14}	-0.000018	-0.000018	-0.000018
a_2	0.0	0.0	-0.023
a_6	0.0	0.0	0.00029
a_{10}	0.0	0.0	0.0000011
a_{14}	0.0	0.0	-0.00000002

Table 10: Comparison of 2D calculation of multipole components in the HGQ magnet body [10] with those obtained from the integrated multipoles in the interval z_p=-50 cm, z_q=-49 cm using the 3D lead and return end models.

In order to assess the accuracy of the 3D field quality calculations presented above, a first consistency check can be performed by comparing the results of a 3D calculation of the integrated multipoles in an interval well inside the magnet body with those of a 2D analysis [10] carried out under the same assumptions (conductors aligned to the outer coil radius, circular iron yoke with inner radius of 9.256 cm and infinite permeability). Table 10 reports the results of such a comparison for the ROXIE-BEND model. The integration limits for the 3D calculation were [-50,-49] cm for both the lead and the return end. Each field integral has been evaluated by adding up the contributions calculated at 1 mm intervals along z. As can be seen, a very good agreement is observed for the return end, while for the lead end small discrepancies are observed. These errors are mainly due to an imperfect positioning of some conductors in those blocks which must be split and defined separately in order to model the coil leads, splices etc. (see figure 3, 5).

Parameter	ROXIE	FIGENDS	Δ_{FR}
L_m (cm)	20.86	20.86	0.0
$\hat{b}_2$	10000	10000	
$\hat{b}_6$	0.082	0.129	0.047
$\hat{b}_{10}$	-0.00626	-0.00617	0.00009
$\hat{b}_{14}$	-0.000018		

Table 11: Integrated harmonic coefficients for the HGQ return end. The integration interval starts at z=-14 cm and ends at z=+20 cm.

Parameter	ROXIE	FIGENDS	Δ_{FR}
L_m (cm)	29.79	29.47	-0.32
$\hat{b}_2$	10000	10000	
$\hat{b}_6$	0.82	0.67	-0.15
$\hat{b}_{10}$	-0.0045	-0.0051	-0.0006
$\hat{b}_{14}$	-0.000014		
$\hat{a}_2$	58.6	61.5	2.9
$\hat{a}_6$	0.034	-0.051	-0.085
$\hat{a}_{10}$	-0.00149	-0.00148	0.00001
$\hat{a}_{14}$	0.000009		

Table 12: Integrated harmonic coefficients for the HGQ lead end. The integration interval starts at z=-24 cm and ends at z=+20 cm.

Table 11 and 12 report a comparison between the magnetic length and the integrated multipole components calculated over the whole end regions using the ROXIE-BEND model and the corresponding values computed using FIGENDS and reported in [6]. In order to carry out a consistent comparison, the integration intervals have been adjusted to match the FIGENDS calculation: [-24,+20] cm for the lead end and [-14,+20] cm for the return end. Although these intervals are shorter than the ones previously considered, they are still sufficiently wide to ensure that the longitudinal field at the extremes is zero with good approximation. First, it should be noted that the result from the 3D ROXIE analysis for the gradient transfer function in the magnet body (table 10) is 18.22 T/m/kA, while the FIGENDS result is 18.51 T/m/kA. This may depend on the model used to distribute the current density in the cable cross-section. For what concerns the magnetic length, the results for the return end are identical (but they are referred to different transfer functions in the straigth section), while in the lead lend a difference of 0.3 cm is observed. The latter may be partly explained by differences in the model geometry, since the length of the leads and the length of the coil splice are not specified in the BEND coordinate files. For what concerns the integrated multipoles, it should be noted that in some cases the integral is obtained as sum of local contributions of rather large amplitude and opposite sign: this situation tends to amplify the dependence of the results on the choice of parameters like the number of current filaments, the length of the integration steps, the number of conductor cross-sections used to describe the end geometry.

The calculation results will eventually be validated by comparison with magnetic measurements carried out on model magnets. The magnetic measurement system is based on rotating coils designed to extract the multipole field components of the field integral calculated over the longitudinal length of the probe. Therefore, its operation is based on equation 2. In the magnet straight section, where the field does not depend on z, the measured $\hat{B}_n$, $\hat{A}_n$ values are related to the B_n, A_n components through the simple relations:

$$B_n = \frac{1}{(z_q - z_p)} \hat{B}_n^{[z_p,z_q]} \qquad A_n = \frac{1}{(z_q - z_p)} \hat{A}_n^{[z_p,z_q]} \tag{6}$$

In the end regions, the measured values can be directly compared with the results in table 8 and 9, provided that the probe extends longitudinally over the whole end region. Some adjustment may be necessary to match the starting point of integration z_p. This can be easily done based on the 2D multipole components in the magnet body.

In order to measure the longitudinal field variation, scans along the z axis are sometimes performed, using either a short probe or the differential results from a long probe which extends well into the magnet straight section. To provide a reference to these measurements, the integrated multipole components have been calculated in a sequence of short consecutive intervals (once again, it should be stressed that these values are in general not suitable to study the local field effect on the beam). For this purpose, the integrated multipole componenents are most conveniently expressed in terms of "units" of 10^{-4} of the integral of the main quadrupole field B_2 *in the straight section* extended over the same physical length:

$$\begin{aligned} \bar{b}_n^{[z_p,z_q]} &= \frac{1}{B_2(z_q - z_p)} \hat{B}_n^{[z_p,z_q]} \cdot 10^4 \\ \bar{a}_n^{[z_p,z_q]} &= \frac{1}{B_2(z_q - z_p)} \hat{A}_n^{[z_p,z_q]} \cdot 10^4 \end{aligned}$$

The $\bar{b}_n$ and $\bar{a}_n$ components as function of z for the orders n=2, 6, 10 in the lead and return end are reported in figures 11 to 16. They have been calculated using integration intervals $[z_p, z_q]$ of 0.2 cm, extending in the range [-25,+25] cm for the return end and [-35,+25] cm for the lead end. Each field integral has been evaluated by adding up the contributions calculated at 1 mm intervals along z.

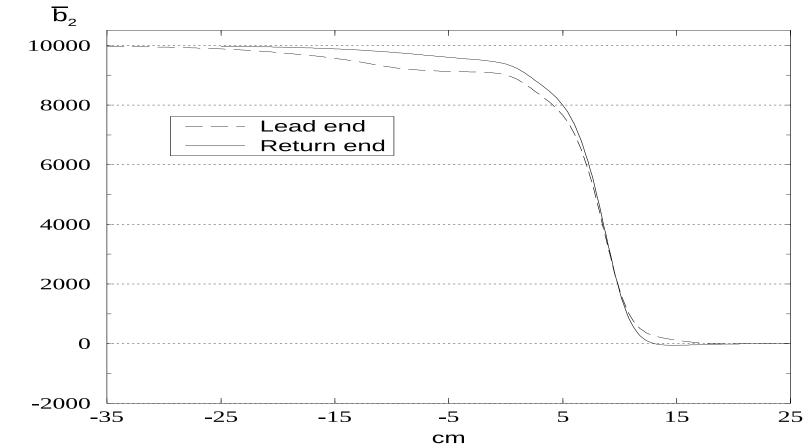

Figure 11: $\bar{b}_2$ in the lead and return end.

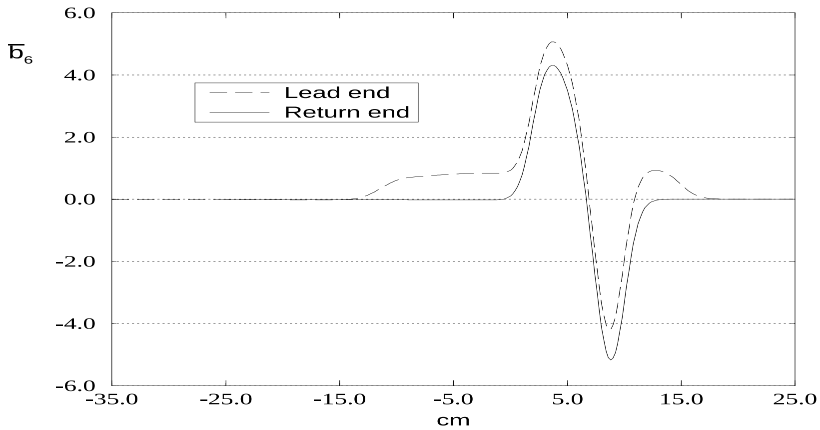

Figure 12: $\bar{b}_6$ in the lead and return end.

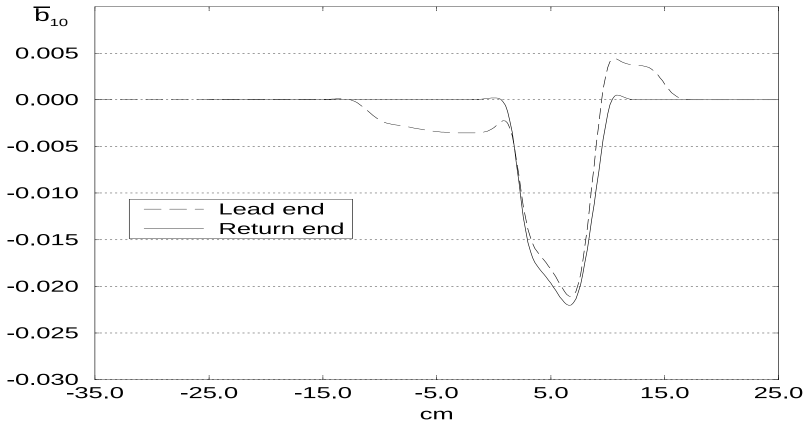

Figure 13: $\bar{b}_{10}$ in the lead and return end.

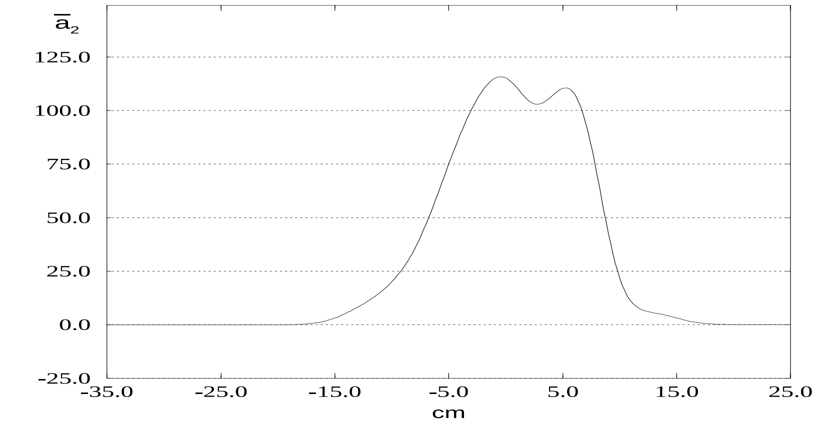

Figure 14: $\bar{a}_2$ in the lead end.

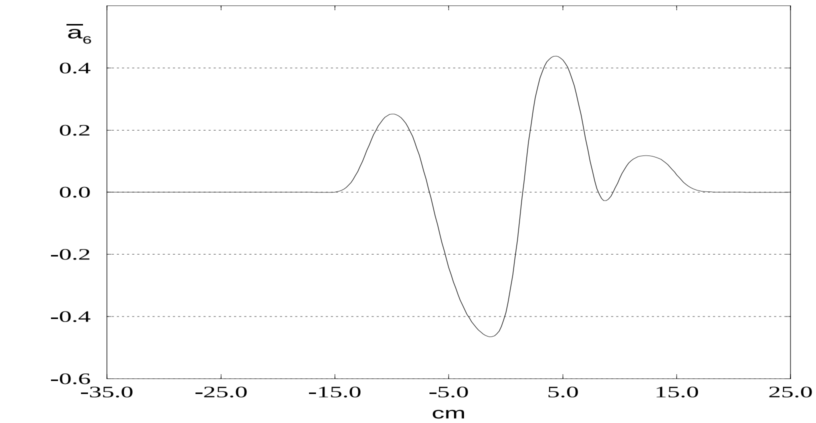

Figure 15: $\bar{a}_6$ in the lead end.

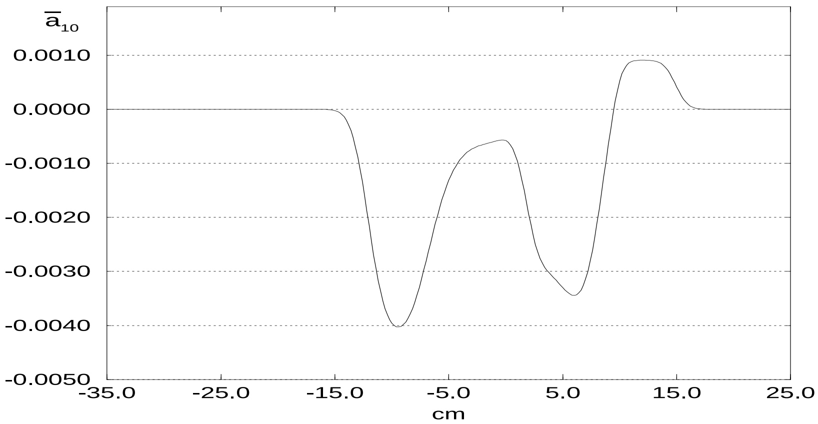

Figure 16: $\bar{a}_{10}$ in the lead end.

6 Conclusions

A magnetic field analysis of the HGQ baseline design for the lead and return coil ends has been presented. The calculations have been performed using ROXIE and the model has been defined using the new BEND-ROXIE interface. The results have been compared with those obtained in previous studies: for what concerns the peak field and the Lorenz forces, substantial agreement has been found, while for what concerns the field quality some discrepancies are observed, which will require further investigation. The results of the field quality calculations have been presented in terms of multipole field components integrated over the whole end regions. These are suitable for comparison with magnetic measurements and for beam tracking studies in which the local field variation is neglected. In order to allow more detailed beam tracking studies keeping into account the local field variation, the values of the magnetic field components on a cylindrical surface inside the magnet bore have been stored and are available upon request.

References

[1] S. Caspi, *"LHC IR Quad"*, FNAL/LBL/CERN videoconference meeting, May 1st, 1996.

[2] J. Brandt, A, Simmons, *"Coil End Design for the LHC IR Quadrupole Magnet"*, Fermilab TS-96-013, November 1996.

[3] J. Cook, *"Strain Energy Minimization in SSC Magnet Winding"*, IEEE Transactions on Magnetics, vol. 27, pp. 1976-1980, March 1991.

[4] G. Sabbi, *"Load lines and short sample limits for HGQ model S01"*, Fermilab TD-97-011, April 1997.

[5] G. Sabbi, *"Calculation of the Longitudinal Lorentz Forces in the Return End of the HGQ"*, Fermilab TD-97-010, March 1997.

[6] S. Caspi, K. Chow, *"Normal and Skew Multipoles in the LHC Low Beta Quad - Rev. 1"*, LBL SC-MAG-577, February 1997.

[7] S. Russenschuck, *"A computer program for the design of superconducting accelerator magnets"*, Proc. ACES Symposium, Monterey, California, 1995 and CERN AT/95-39, September 1995.

[8] S. Caspi, M. Help, L. Laslett, *"3D Field Harmonics"*, LBL Report SC-MAG-328, March 1991.

[9] S. Caspi, M. Helm, L. Laslett, V. Brady, *"An approach to 3D Magnetic Field Calculation Using Numerical and Differential Algebra Methods"* LBL SC-MAG-395, July 1992.

[10] G. Sabbi, A. Zlobin, *"Field Errors in the HGQ Straight Section"*, Fermilab TD-97-012, June 1997.